Conceptual Design for a 1-GeV IFEL Accelerator

W. D. Kimura[*], P. Musumeci[†], D. C. Quimby[*], S. C. Gottschalk[*], and C. Pellegrini[†]

[*]*STI Optronics, Inc., 2755 Northup Way, Bellevue, WA 98004*
[†]*University of California, Los Angeles, Los Angeles, CA 90095*

Abstract. A conceptual design for a multistaged 1-GeV IFEL laser-driven accelerator (laser linac) was developed using the Staged Electron Laser Acceleration (STELLA) inverse free electron laser (IFEL) model created at STI Optronics. A comparison with the UCLA TREDI model yields good agreement with the STELLA model. The 1-GeV IFEL laser linac consists of an IFEL buncher for forming microbunches and four IFEL acceleration stages. Electrons enter the laser linac from a conventional microwave-driven linac (51 MeV). The acceleration stages are driven by 10-TW laser beams at 1.06-μm. It is found good trapping occurs as the electrons are accelerated; however, refocusing of the *e*-beam between acceleration stages is needed to control detrapping effects. The energy spread of the trapped electrons is also small. This design exercise was in support of the task placed upon the EM Structure-Based Accelerators Working Group at the 2004 Advanced Accelerator Concepts Workshop. It demonstrates that a 1-GeV IFEL laser linac is feasible with present technology.

INTRODUCTION

Inverse free electron lasers (IFEL) [1], [2] are one of the most mature of the various laser-driven acceleration methods. At UCLA, high energy gains (>150%) and high acceleration gradients (>70 MeV/m) have been demonstrated [3]. During the Staged Electron Laser Acceleration (STELLA) program at the Brookhaven National Laboratory Accelerator Test Facility (ATF), efficient trapping and acceleration of IFEL-generated microbunches with narrow energy spread (i.e., monoenergetic) have also been shown [4]. Staging between IFEL devices has been done [5], which is important for building up an accelerator system. Hence, many of the key capabilities needed for constructing a laser-driven accelerator system (laser linac) have been demonstrated for IFELs.

In addition to these experimental accomplishments, IFEL computer models have been developed at STI Optronics (STI) [6] and UCLA [7], and validated against the data. These permit designing an IFEL accelerator system with high confidence.

Thus, in response to the charge given to the 2004 EM Structure-Based Accelerators Working Group (WG) to develop conceptual designs for a 1-GeV accelerator, the authors were asked by the WG Leaders to develop an initial "strawman" design for a 1-GeV IFEL laser linac to present to the WG. Such a device might be useful as a compact, potentially less expensive linac. The high peak power due to the inherently

CP737, *Advanced Accelerator Concepts: Eleventh Workshop,*
edited by Vitaly Yakimenko

short microbunch lengths produced by an IFEL may also make them particularly attractive as drivers for Self-Amplified Spontaneous Emission (SASE) free electron lasers (FEL).

This paper describes this strawman design and related issues.

MODELING ASSUMPTIONS, PROCEDURE, AND RESULTS

Due to limited time and resources, the modeling effort had to be restricted in scope and depth. The STI STELLA model [6] served as the primary tool with the UCLA TREDI model [7] used to confirm the results of the STELLA model. A separate STI code was used to produce the proper taper prescription for the wigglers to maintain the FEL resonance condition along the wiggler as the electrons gained energy for a given driving laser intensity. Both the magnetic field strength and magnetic period are tapered. The STELLA model then uses the tapered magnetic field for each wiggler in its calculations. Transverse field roll-off is not included in these calculations.

Certain parameters were preselected and specific assumptions made in order to simplify this effort. These parameters and assumptions are listed in Tables 1 and 2, respectively. We believe the parameter values are realistic ones, but they have not been optimized. Therefore, the design presented in this paper should be viewed as only a representative one. The assumptions define the limits of this design exercise.

The first device in the laser linac is the IFEL buncher. This uses an untapered wiggler because only a small amount of energy modulation is needed. This also means the exact parameter values of the buncher are not critical since one can trade off number of wiggler periods, wiggler length, and laser intensity to achieve the same amount of modulation. A chicane is also not needed because of the 100-cm drift space between the buncher and first acceleration stage, which allows bunching to occur.

TABLE 1. Fixed system parameters for 1-GeV IFEL accelerator design.

Parameter	Fixed Value	Comments
Initial *e*-beam energy (γ value)	51.1 MeV (γ = 100)	Typical of ATF-like linac.
Initial *e*-beam intrinsic energy spread	0.03% (1σ)	Typical of ATF-like linac.
Laser wavelength	1.06 μm	10.6 μm still viable candidate.
Laser peak power driving accelerator stages	10 TW	Readily available from solid-state lasers.
Nominal length of accelerator wigglers	≤100 cm	Actual length varies slightly (see text).
Rayleigh range within accelerator wigglers	20 cm	For 1.06-μm wavelength, means waist radius is 0.26 mm.
Location of laser waist inside wigglers	50 cm	In center of wiggler.
Separation distance between all stages, including buncher	100 cm	May need to be longer to avoid damaging mirrors (see text).
Resonant phase angle ψ for wigglers	ψ = 30°	Compromise between good acceleration and good trapping.

TABLE 2. Assumptions made for 1-GeV IFEL strawman design.

Parameter	Assumption and Comments
Emittance	$\varepsilon_n = 10^{-6}$ mm-mrad. Near-zero value means the *e*-beam is essentially a "pencil-beam" with no appreciable *e*-beam focusing effects along the linac system. Exception is in wiggle plane where other effects can cause the *e*-beam trajectory to deviate away from the longitudinal axis.
Temporal effects	Laser and *e*-beam temporal profiles are ignored. Essentially this means the beam profiles are idealized "top-hat" ones. It is also assumed the electrons experience the same laser peak power, but at different phases.
Spatial overlap	Perfect spatial overlap of the *e*-beam and laser within the buncher is assumed; however, it is not necessarily true in the subsequent acceleration stages.
Space-charge	Space-charge effects are ignored. Since for a 1.06-μm laser wavelength, the resultant microbunch length is of order 100 nm, space-charge spreading along the longitudinal direction can quickly become an appreciable effect.
Coherent synchrotron radiation (CSR)	CSR is ignored. Can be important for ultra-short *e*-beam pulses and/or high *e*-beam charge.
Synchrotron radiation losses	Model calculations show loss is negligible for 1-GeV beam.
Laser beam energy depletion	Assume negligible depletion of laser beam energy while interacting with electrons. Becomes nonnegligible for high beam charge and energy gain.

For a given input *e*-beam energy, the tapered prescription code gives the predicted output energy and the tapered magnetic field. Using the tapered magnetic field, the STELLA model yields the *e*-beam characteristics exiting the stage. This process is repeated for each stage where the output *e*-beam parameters from the previous stage are used as the input to the next stage. The taper prescription code is also run for the next stage since the amount of taper changes because the input energy is now higher.

Figure 1 shows the overall layout for the 1-GeV IFEL laser linac and summarizes the model predictions for each stage. Z_R is the Rayleigh range and λ_w is the wiggler period. The laser beams reflect off mirrors into the wigglers with a small hole in the

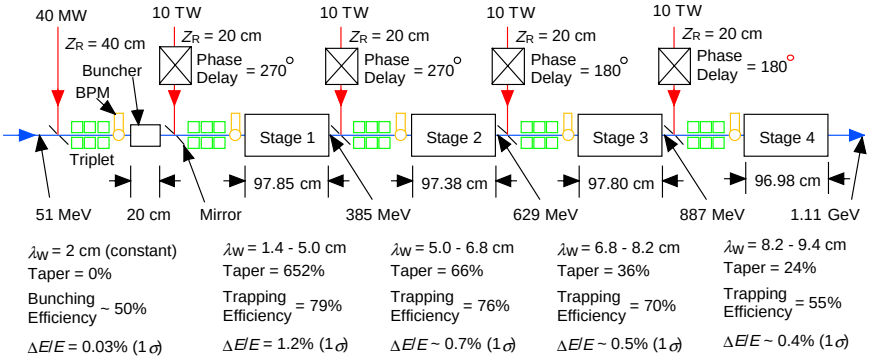

FIGURE 1. Layout for 1-GeV IFEL laser linac and predicted *e*-beam characteristics after each stage.

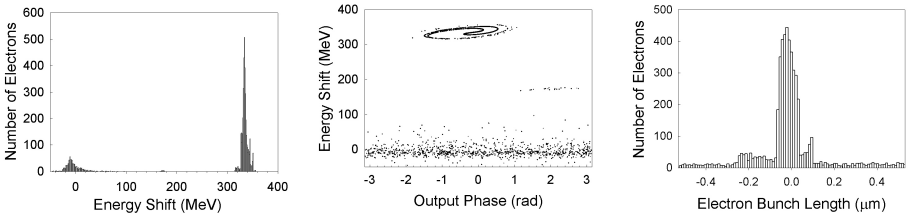

(a) (b) (c)

FIGURE 2. STELLA model predictions for Stage 1. (a) Energy shift from initial energy, i.e., 51.1 MeV. (b) Energy-phase diagram. (c) Longitudinal density distribution of electrons.

mirrors enabling transmission of the *e*-beam. Although *e*-beam focusing triplets are depicted in Fig. 1, these were not included in the modeling. Instead the ultralow emittance keeps the *e*-beam diameter small in the nonwiggle plane of the wiggler. In the wiggle plane, spreading of the *e*-beam does occur, which, as discussed later, leads to detrapping of the microbunch electrons out of the accelerating ponderomotive potential well ("bucket"). Usage of the triplets would normally compensate for this *e*-beam spreading, thereby, controlling detrapping.

Only 40 MW of laser power into the 20-cm buncher wiggler is needed to achieve good microbunches at the entrance to the 1st acceleration stage (Stage 1). The bunching efficiency is 50%, which is typical for sinusoidal modulation.

Stage 1 has the greatest taper amount of 652% (defined as the change in resonant γ) with its wiggler period changing from 1.4 cm to 5.0 cm. This large amount of taper is not unprecedented; the UCLA wiggler had 250% taper, and was both wavelength and field tapered. The average acceleration gradient for Stage 1 is 340 MeV/m.

Figure 2(a) is the energy histogram for Stage 1 and shows a well-separated group of electrons with >330 MeV energy gain, an energy spread of about 1.2% (1σ), and 79% of the initial electrons. Both theory [8] and experiments [4] have shown that trapping efficiencies approaching 80% are possible.

The energy-phase plot corresponding to Fig. 2(a) is given in Fig. 2(b). A well-defined ellipse of trapped electrons can be seen with the untrapped and unaccelerated electrons remaining randomly distributed over all phase near zero energy gain.

Figure 2(c) shows the microbunch longitudinal profile derived from Fig. 2(b). The microbunch length is about 0.1 μm and similar to the length produced by the buncher.

Note in Fig. 1 that the length of the 1st stage is not exactly 100 cm. This length was chosen to maintain zero deflection of the *e*-beam transiting the wiggler. An actual wiggler would be designed with partial strength end magnets and steering coils to achieve zero deflection. It was easier in this simple effort to adjust the wiggler length.

Figures 3-5 give the analogous model results for Stages 2, 3, and 4. The amount of taper is lessening with each stage. The gradient is also decreasing to 262, 232, and 215 MeV/m for Stages 2, 3, and 4, respectively.

A narrow energy spread of the trapped electrons is being maintained and appears to be less than 1%. However, the finite width of the energy spectrum histogram bars makes it difficult to accurately estimate this width.

The trapping efficiency from stage to stage is also dropping. Detrapped electrons can be clearly seen in the phase plots [Figs. 3(b), 4(b), and 5(b)] lying between the unaccelerated electrons and the phase ellipse. Preliminary analysis indicates these detrapped electrons are ones that have been deflected away from the center axis in the wiggle plane. Without focusing triplets there is no means in the model to bring these electrons back on axis before they enter the next stages. Nonetheless, even under these nonoptimized conditions, Fig. 5 indicates that an appreciable amount of electrons can be accelerated to 1 GeV while preserving a narrow energy spread and short microbunch length.

The TREDI model gave similar results for trapping efficiency and energy gain.

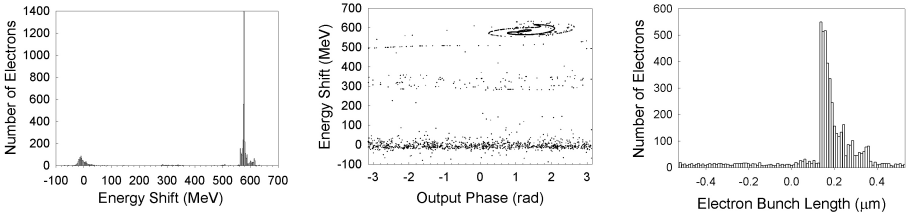

(a) (b) (c)

FIGURE 3. STELLA model predictions for Stage 2. (a) Energy shift from initial energy. (b) Energy-phase diagram. (c) Longitudinal density distribution of electrons.

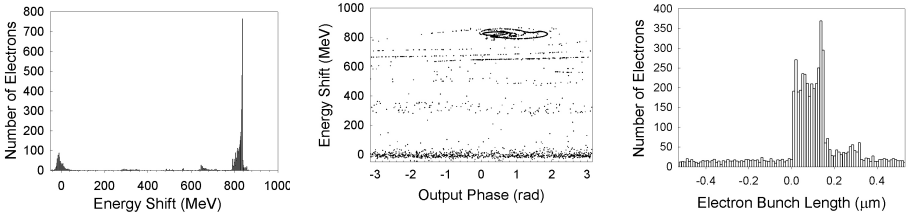

(a) (b) (c)

FIGURE 4. STELLA model predictions for Stage 3. (a) Energy shift from initial energy. (b) Energy-phase diagram. (c) Longitudinal density distribution of electrons.

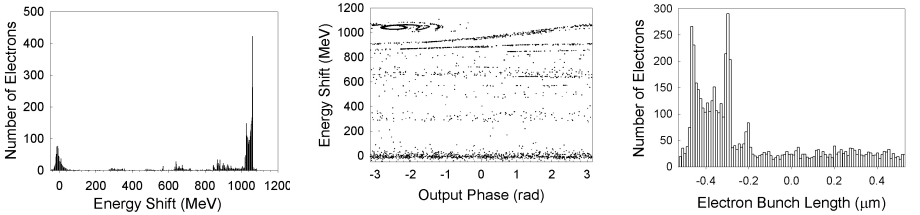

(a) (b) (c)

FIGURE 5. STELLA model predictions for Stage 4. (a) Energy shift from initial energy. (b) Energy-phase diagram. (c) Longitudinal density distribution of electrons.

DISCUSSION

Mirror Damage Issues

Optical damage of the mirror used to direct the laser beam into the wigglers (see Fig. 1) is an important constraint. Assuming the mirror is positioned 100 cm from the wiggler, then for 10-TW laser power and Z_R = 20 cm, the laser intensity on the 45° mirror is 3.8×10^{14} W/cm^2. Typical 10-TW lasers have pulse lengths of order 30 fs. For this pulse duration the fluence on the mirror is 8 J/cm^2, which is about 4 times beyond the damage limit.

There are different ways to reduce the fluence: 1) Shortening the laser pulse (e.g., ≤7 fs), which may not be feasible. 2) Decreasing Z_R, which also reduces the laser beam waist size and requires tighter *e*-beam focusing. It also departs from the optimum Rayleigh range for driving the IFEL [9]. 3) Operate the turning mirror at glancing incidence using multiple mirrors in a "whispering-gallery" arrangement. Or, 4) increasing the distance between the stages to move the mirror further away from the wiggler. This last approach is the easiest to implement. A separation distance of 200 cm would decrease the fluence to 2 J/cm^2 and result in a total laser linac length of ≈13 m (not including the microwave-driven 51-MeV linac).

Ultrashort Laser Pulse Issues

By design, the electrons at resonance in an IFEL slip one optical period λ_L per magnet period λ_M. Hence, for λ_L = 1.06 μm, the electrons slip out of a 30-fs laser pulse (≡9 μm) in <9 magnet periods. The number of periods of the wigglers in Fig. 1 range from 11 to 31. Hence, they have too many periods for a 30-fs laser pulse. One remedy is to use 8-period wigglers and increase the number of stages. This makes the system more complex, but it is still doable.

A more fundamental issue is the laser pulse length should be greater than the *e*-beam pulse length so that the electrons experience nearly the same optical field. Thus, a 30-fs laser pulse implies the need for, say, a few femtosecond *e*-beam pulse. Such a short *e*-beam pulse may be difficult to deliver and would be severely limited by space charge effects. Note if the *e*-beam pulse is longer than the laser pulse, then this simply means less charge will be accelerated by the IFEL system.

A given laser pulse length τ_L has opposing consequences. A short pulse favors higher peak power and increase optical damage limit; whereas, a long pulse favors a longer *e*-beam pulse length. A longer *e*-beam pulse enables higher charge, less problems with CSR, and usage of more periods in the wigglers.

One can work the design analysis backwards starting with the minimum desired charge. This implies a minimum *e*-beam pulse length τ_e, which implies a minimum laser pulse length, say, $\tau_L = 10\tau_e$. This implies a maximum number of wiggler periods N_{max}, i.e., $N_{max} = \tau_L c/\lambda_L$, where c is the speed of light. It also implies a minimum laser pulse energy to achieve the needed peak power. This pulse energy sets the minimum distance for the turning mirror and the separation distance between stages. Hence, the separation distance may dominate the total length of the IFEL laser linac.

1.06-μm Versus 10.6-μm Lasers

A brief comparison between using a 1.06-μm laser to drive the IFEL versus a 10.6-μm laser can be made. This comparison is not an exhaustive one and is presented primarily to give a flavor of the complexities of this issue.

Short laser wavelength pros are: 1) very high peak power (~100 TW) and high intensities because of tight focusing with short wavelengths; 2) good pulse repetition rates (e.g., 10 Hz); 3) table-top-sized laser systems; and 4) high-damage-threshold optics available. Cons are: 1) need ultrashort *e*-beam pulses or must accept less accelerated charge; 2) ultrashort microbunches (e.g., ~100 nm), which are more susceptible to space charge spreading and CSR effects; 3) limit to number of wiggler periods (ultrashort τ_L offsets short λ_L in $\tau_L c/\lambda_L$ ratio); 4) small laser waist requires very tight *e*-beam focusing and very low emittance; and 5) alignment and stability more difficult with short wavelengths.

Long laser wavelength pros are: 1) longer microbunches, which are less susceptible to space charge spreading and CSR effects; 2) more wiggler periods possible (relatively long τ_L compensates for long λ_L in $\tau_L c/\lambda_L$ ratio); 3) larger laser waist easing *e*-beam focusing requirements; and 4) alignment and stability easier. Cons are: 1) peak power and intensity lower than solid-state lasers; 2) repetition rate limited, but can increase by flowing gas; 3) high-pressure CO_2 laser amplifiers large in size; and 4) total length of IFEL laser linac will be longer because acceleration gradient is smaller.

CONCLUSION

A first-order conceptual design for a 1-GeV IFEL laser linac was developed attempting to use realistic parameter values. This exercise shows that such a system is feasible with present technology; however, many ancillary issues must still be examined.

ACKNOWLEDGMENTS

This work was sponsored by the Work was supported by the U.S. Department of Energy, Grant Nos. DE-FG02-04ER41294 and DE-FG02-92ER40693.

REFERENCES

1. R. B. Palmer, J. Appl. Phys. **43**, 3014 (1972).
2. E. D. Courant, C. Pellegrini, and W. Zakowicz, Phys. Rev. A **32**, 2813 (1985).
3. P. Musumeci, "Very High Energy Gain at the Neptune IFEL Experiment," in these Proceedings.
4. W. D. Kimura, *et al*., Phys. Rev. Lett. **92**, 054801 (2004).
5. W. D. Kimura, *et al*., Phys. Rev. Lett. **86**, 4041 (2001).
6. W. D. Kimura, *et al*., Phys. Rev. ST Accel. Beams **4**, 101301 (2001).
7. L. Giannessi, P. Musumeci, M. Quattromini, NIM A **436**, 443 (1999).
8. D. C. Quimby, C. G. Parazzoli, and D. J. Pistoresi, Nucl. Inst. Meth. Phys. Res. A318, 628 (1992).
9. P. Musumeci, "Acceleration of Electrons by Inverse Free Electron Laser Interaction," Ph.D. thesis, UCLA, 2004, p. 30.